EPJ Web of Conferences **123**, 03006 (2016) DOI: 10.1051/epjconf/201612303006
Heavy Ion Accelerator Symposium 2015

Mass-asymmetric fission in the ^{40}Ca+^{142}Nd reaction

E. Prasad[1,a,b], D. J. Hinde[1], E. Williams[1], M. Dasgupta[1], I. P. Carter[1], K. J. Cook[1], D. Y. Jeung[1], D. H. Luong[1], S. McNeil[1], C. S. Palshetkar[1], D. C. Rafferty[1], C. Simenel[1], A. Wakhle[1,c], K. Ramachandran[1,d], J. Khuyagbaatar[2,e], Ch. E. Dullmann[2,f], B. Lommel[2], and B. Kindler[2]

[1]*Department of Nuclear Physics, Research School of Physics and Engineering, Australian National University, Canberra, ACT 2601, Australia.*
[2]*GSI Helmholtzzentrum fur Schwerionenforschung, 64291, Darmstadt, Germany.*

Abstract. Shell effects play a major role in fission. Mass-asymmetric fission observed in the spontaneous and low energy fission of actinide nuclei was explained by incorporating the fragment shell properties in liquid drop model. Asymmetric fission has also been observed in the low energy fission of neutron-deficient ^{180}Hg nuclei in recent β-delayed fission experiments. This low-energy β-delayed fission has been explained in terms of strong shell effects in pre-scission configurations associated with the system after capture. Calculations predicted asymmetric fission for heavier Hg isotopes as well, at compound nuclear excitation energy as high as 40 MeV. To explore the evolution of fission fragment mass distribution as a function of neutron and proton numbers and also with excitation energy, fission fragment mass distributions have been measured for the ^{40}Ca+^{142}Nd reaction forming the compound nucleus ^{182}Hg at energies around the capture barrier, using the Heavy Ion Accelerator Facility and CUBE spectrometer at the Australian National University. Mass-asymmetric fission is observed in this reaction at an excitation energy of 33.6 MeV. The results are consistent with the β-delayed fission measurements and indicate the presence of shell effects even at higher exciation energies.

1 Introduction

Nuclear fission is a dynamic process involving large scale collective motion, often affected by a subtle interplay of macroscopic and microscopic effects during the transition of the fissioning nucleus from its ground state deformation to the scission point. Fragment mass distributions are an important observable in fission which provides crucial information about the potential-energy landscape of the fissioning system. Fragment mass distributions have been observed to be predominantly asymmetric in the spontaneous or low energy fission of most of the actinide nuclei [1], which could not be explained solely by using the liquid drop model (LDM) [2]. The experimental observations were explained by incorporating the fragment shell properties near the scission configuration, particularly the spherical shell closure (Z = 50, N = 82) or deformed neutron shells (N = 88) [1, 3], within the LDM frame work.

Recent observations of mass-asymmertic fission of the Hg isotopes in β-delayed fission experiments [4, 14] indicated the role of shell structures other than fragment shells in deciding the fission outcomes. The low yield of symmetric fission in ^{180}Hg populating ^{90}Zr (Z = 40, N = 50) led to the speculation that fragment shell effects, though significant in the potential energy surface near scission, must not play a major role in determining the mass split in this nucleus.

Even though β-delayed fission experiments allowed us to access the low energy fission regime of the neutron-deficient nuclei in the mass 180-200 region, the availability of nuclei undergoing this process is severely limited by the stringent conditions on β-decay Q-values and branching ratios [4]. Also, the maximum available excitation energy for the fissioning system is restricted by the Q-value of the parent nucleus [4]. In the actinide region, it is observed that [1, 5] the fragment mass division becomes symmetric with increasing excitation energy, as shell effects generally wash out at higher excitations. In order to understand the evolution of fission fragment mass distribution as a function of neutron and proton numbers (N and Z) of the fissioning system and the excitation energy in the neutron deficient Hg region, we measured the fission fragment mass distributions of ^{182}Hg populated through the fusion reaction ^{40}Ca+^{142}Nd at energies around the capture barrier. The results are compared with the latest experimental data available in the same mass region for the fis-

[a]e-mail: prasad.edayillam@anu.edu.au
[b]Permanent Address: Department of Physics, Central University of Kerala, Kasaragod, 671314, India.
[c]Presently at National Superconducting Cyclotron Laboratory, Michigan State University, Michigan, 48824, USA.
[d]Presently at Bhabha Atomic Research Center, Mumbai 400085, India.
[e]Helmholtz Institute Mainz, 55099 Mainz, Germany.
[f]Institute for Nuclear Chemistry, Johannes Gutenberg University Mainz, 55128 Mainz, Germany.

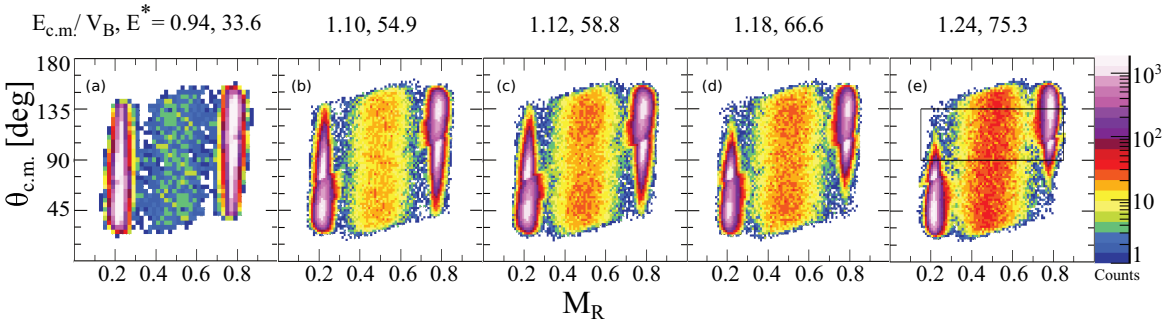

Figure 1. Experimental MAD scatter plots for the ^{40}Ca+^{142}Nd reaction at different beam energies. The $\frac{E_{c.m.}}{V_B}$ values and CN excitation energies E^* are given at the top of each plot. E^*, $E_{c.m.}$ and V_B are in units of MeV.

sion of different Hg isotopes and also with the predictions of some of the theoretical calculations available.

2 Experimental details and data analysis

The experiment was performed using the 14UD Pelletron accelerator and superconducting linear accelerator facility at the Australian National University. Pulsed ^{40}Ca beams with a pulse seperation of 106.7 ns and full width at half-maximum (FWHM) of 0.7-1.5 ns were used to bombard the isotopically enriched $^{142}NdF_3$ target of thickness 400 μg/cm^2, with a 18 μg/cm^2 carbon backing facing downstream. The measurements were performed at 167.7, 194.9, 199.9, 210.0 and 221.1 MeV laboratory energies and the fission fragments were detected using the CUBE [6] fission spectrometer. CUBE consists of two large area position sensitive multiwire proportional counters, each with an active area of 279 × 357 mm^2. These detectors were mounted at 45° and 90° scattering angles with respect to the beam direction, such that the normal to the central foil of both detectors was at 180 mm from the center of the target. The target normal was oriented at 60° with respect to the beam axis to avoid shadowing of the detectors. Two silicon monitor detectors were mounted at $\theta = 30°$, at azimuthal angles of 90° and 270°, to detect the elastically scattered beam particles.

The CUBE detectors provide timing, position, and energy loss signals of the particles entering them. The calibrated position and time of flight information were used to obtain the fragment velocities and center-of-mass angles. The mass ratio (M_R) of the fragments is then obtained as,

$$M_R = \frac{m_1}{m_1 + m_2} = \frac{v_2}{v_1 + v_2} \quad (1)$$

where m_1 and m_2 are the masses of fragments at scission and v_1 and v_2 are their center-of-mass velocities, respectively. Light particle evaporation from the fragments does not alter the centroids of the M_R distribution, as the mass ratio is derived from the fragment velocities, which - on average - are not affected by the evaporation of light particles.

Mass-angle distribution (MAD) plots [7] of the fragments provide a direct indication of the presence of processes other than fusion-fission in heavy ion reactions. MAD plots generally consist of groups originating from elastic, inelastic, fusion-fission and quasifission processes. Unlike the elastic and inelastic events, quasifission events overlap significantly with those from the fusion-fission making their separation impossible in most cases. However, in general, a strong component of quasifission may be inferred from the presence of mass-angle correlations in a MAD plot [7].

3 Results

MADs of the fragments were generated to probe the presence of processes other than fusion-fission in the ^{40}Ca+^{142}Nd reaction and are shown in Fig. 1. The $\frac{E_{c.m.}}{V_B}$ values and compound nucleus (CN) excitation energies (E^*) are given at the top of each plot, where $E_{c.m.}$ is the center-of-mass energy and V_B is the capture barrier from a calculation [8] optimised for heavy systems. Since we detect both the fragments in our experimental setup, the MAD is populated twice, at (M_R, $\theta_{c.m.}$) and (1 − M_R, π-$\theta_{c.m.}$). Hence the MAD plots shown in Fig. 1 are suitably mirrored. The non-appearance of a strong correlation in fragment mass and emission angle in the MAD for the ^{40}Ca+^{142}Nd reaction indicates the absence of fast quasifission originating from quick re-separation of the di-nuclear system after capture in this reaction. The M_R

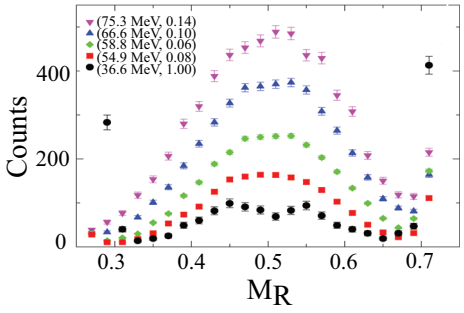

Figure 2. The fission M_R distributions from the ^{40}Ca+^{142}Nd reaction at different CN excitation energies as indicated. The yields are scaled to show all energies in a single plot, scaling factors are shown inside the parantheses.

distributions of the fragments were obtained by projecting these MADs onto the M_R axis. An angular window ($\Delta\theta$) of 45° [90° ≤ $\Delta\theta$ ≤ 135° as indicated in Fig. 1 (e)] has been selected to avoid the biasing of the data due to the geometrical limits of the detector and also to eliminate any mirrored data in the final M_R distribution.

The experimental M_R distributions for the ^{40}Ca+^{142}Nd reaction at different CN excitation energies (E^*) are shown in Fig. 2. A strong mass-asymmetric component is observed in the M_R distribution at E^*=33.6 MeV. The M_R distributions at higher excitation energies do not show any direct signature of mass-asymmetric fission and can be represented by a single flat-topped Gaussian function.

The width of the fragment M_R distribution is obtained by fitting the distribution with a single Gaussian function. The standard deviations (σ_{MR}) of the Gaussian fit at different CN excitation energies are shown in Table 1. The σ_{MR} values increase with increasing excitation energy. Even though the absence of mass-angle correlation rules out fast quasifission in the ^{40}Ca+^{142}Nd reaction, quasifission with longer sticking times may be contributing to larger σ_{MR} values ($\sigma_{MR} \geq 0.07$ [7]) observed in this reaction. Slow quasifission could contribute to an increase in mass widths at higher energies and angular momenta, but the smallest contribution is expected at the lowest energy. Because of their longer sticking times in comparison with the fast quasifission events [7], slow quasifission is not expected to produce mass-angle correlations in the MAD plots.

Table 1. Single Gaussian widths (σ_{MR}) obtained for the M_R distributions for the ^{40}Ca+^{142}Nd reaction at different CN excitation energies.

E* (MeV)	σ_{MR}
33.6	0.0862±0.0030
54.9	0.0824±0.0007
58.8	0.0877±0.0006
66.6	0.0950±0.0008
75.3	0.1006±0.0010

4 Discussion

According to a recent macroscopic-microscopic finite-range liquid-drop model calculation [9], the zero angular momentum fission barrier height of ^{182}Hg is 10.85 MeV. Hence, the available excitation energy above the saddle point (E_s^*) for ^{182}Hg nuclei formed in the ^{40}Ca+^{142}Nd reaction is 22.8 MeV at the lowest measured energy. The M_R distributions from the fission of ^{180}Hg, ^{190}Hg and ^{195}Hg populated at similar or nearby excitation energies above the zero angular momentum saddle point, populated through the reactions ^{36}Ar+^{144,154}Sm [10] and ^{13}C+^{182}W [11, 12], respectively, are compared with our

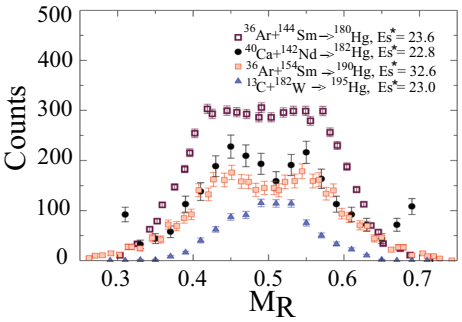

Figure 3. The scaled M_R distributions of fission from different reaction populating isotopes of Hg. The excitation energy available above the zero angular momentum fission barrier (E_s^* in MeV) is also shown.

present observation in Fig. 3. Different parameters of the reactions studied in this paper are given in Table 2. The fragment mass distributions reported in Ref. [10] for the ^{36}Ar+^{144,154}Sm reaction have been converted into M_R distributions in this plot for a direct comparison. It is interesting to note that the fission from ^{180}Hg and ^{190}Hg nuclei produced in the ^{36}Ar+^{144,154}Sm reactions also show signatures of asymmetric mass split. However, a symmetric split has been observed in the fission of ^{195}Hg formed in the ^{13}C+^{182}W reaction, showing a transition from asymmetric to symmetric mass division with increase in neutron number in Hg isotopes. Similarly, a symmetric-peaked distribution has also been reported for the fission of ^{198}Hg [13].

Table 2. The CN produced, CN excitation energy (E^*) and excitation energy available above the zero-angular momentum saddle point (E_s^*) for different reactions studied in this paper.

Reaction	CN	E^* (MeV)	E_s^* (MeV)
^{36}Ar+^{144}Sm [10]	^{180}Hg	33.4	23.6
		39.8	30.0
		47.8	38.0
		65.5	55.7
^{40}Ca+^{142}Nd	^{182}Hg	33.6	22.8
		54.9	44.1
		58.8	48.0
		66.6	55.8
		75.3	64.5
^{36}Ar+^{154}Sm [10]	^{190}Hg	47.8	32.6
		55.9	40.7
		62.4	47.2
		70.5	55.3
^{13}C+^{182}W	^{195}Hg	41.8	23.0
		44.6	25.8
		47.4	28.6

The observation of asymmetric mass division in the low energy fission of ^{180}Hg [4, 14] in β-delayed fission experiments triggered special interest in the fission of

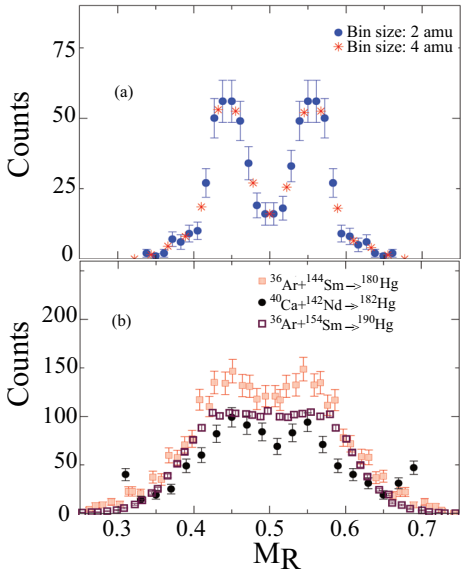

Figure 4. (a) The M_R distributions of ^{180}Hg from the β-delayed fission measurements (E^* = 10.44 MeV). The fragment mass distribution is converted into M_R distribution, with different bin sizes. (b) The M_R distributions of fission from ^{180}Hg (^{36}Ar+^{144}Sm, E^*= 33.4 MeV), ^{182}Hg (^{40}Ca+^{142}Nd, E^*=33.6 MeV) and ^{190}Hg (^{36}Ar+^{154}Sm, E^*= 47.8 MeV).

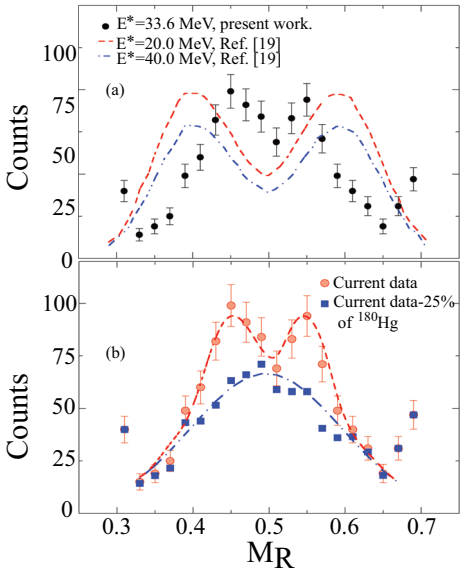

Figure 5. (a) The M_R distributions of fission fragments from the ^{40}Ca+^{142}Nd reaction at E^*=33.6 MeV compared with BSM predictions of ^{182}Hg [19] at E^*=20 and 40 MeV. (b) M_R distribution obtained by subtracting 25% contribution from the fission of ^{180}Hg. A Gaussian fit to this distribution is shown using the dot-dashed line (blue). Dashed line (red) represents the sum of the Gaussian fit values and 25% fission contribution from ^{180}Hg.

nuclei in the neutron deficient Hg region. Soon after this observation, different theoretical explanations were put forward to explain the experimental results. Among these calculations, potential energy surface calculations [4, 15] provided a qualitative explanation of the data and predicted similar observations for heavier isotopes of Hg. Microscopic calculations based on the Skyrme-HFB model [16] also reproduced the experimental observations in ^{180,198}Hg. Calculations based on a modified scission point model [17, 18] also explained low energy fission results observed for ^{180}Hg. Interestingly, though based on different model assumptions, all these calculations reproduced the β delayed fission results reasonably well.

The M_R distributions observed in the ^{40}Ca+^{142}Nd and ^{36}Ar+^{144,154}Sm reactions are thus compared with the results from β-delayed fission in Fig. 4. A striking feature is the similarity in mass division in all these reactions. It is reported that the asymmetric peaks in the fission of ^{180}Hg in Ref. [14] are centered around ^{80}Kr and ^{100}Ru, translating to M_R values 0.46 and 0.54 for the light and heavy fragments, respectively. The M_R peaks observed in the ^{40}Ca+^{142}Nd reaction are also consistent with these values. The peaks of the two Gaussian functions used to represent the mass distributions in the ^{36}Ar+^{144,154}Sm reactions in Ref. [10] also correspond to similar M_R values, consistent with that of β-delayed fission results.

The observation of mass-asymmetric fission in the ^{40}Ca+^{142}Nd fusion-fission reaction appears to support the influence of shell effects up to this excitation energy. The relatively low fissility of ^{182}Hg suggests that the observed fission may be dominated by first chance fission of the CN itself. Fission yield calculations based on Brownian Shape Motion (BSM) by Moller [19] predicted asymmetric fission in Hg isotopes (^{176}Hg to ^{188}Hg) up to CN excitation energies as high as 40 MeV. Similarly, calculations based on finite-temperature density functional theory [20] also predicted the occurrence of mass-asymmetric fission in neutron deficient Hg isotopes at high CN excitation energies up to 30 MeV. We thus compared our results with the BSM predictions for the fission of ^{182}Hg in Fig. 5(a). Though both theoretical predictions and experimental results show similar trends in mass split, the mass centroids of the asymmetric peaks are different. Similar observations may also be made for the low energy [14] and high energy [10] fission of ^{180}Hg. However, the predicted results match with the experimental results for ^{190}Hg [10]. In addition to the mismatch in mass centroids, significant difference in the FWHM of the asymmetric peaks was observed in the experimental results and BSM predictions.

On the other hand, pre-scission neutron multiplicity (ν_{pre}) estimates based on the systematics available in literature (ν_{pre}=0.51 according to the systematics from Ref. [21] and 0.82 from [22]) indicate that multichance fission may be significant in the case of ^{182}Hg, leading to a possibility that low energy fission of ^{180}Hg may be contributing to the observed M_R distribution in the ^{40}Ca+^{142}Nd reaction. Such a possibility is explored by first normalising the area under the M_R distributions from the β-delayed fission study and ^{40}Ca+^{142}Nd reaction at E^*=33.6 MeV and, then, subtracting a fraction of the M_R distribution of ^{180}Hg from that of ^{182}Hg. It was observed

that subtracting a 25% contribution of fission of ^{180}Hg from that measured from the ^{40}Ca+^{142}Nd reaction leads to a distribution which can be represented by a single Gaussian centered at mass symmetry. This is shown in Fig. 5(b). While the dot-dashed curve represents the Gaussian fit to the symmetric distribution, the dashed line represents the sum of this Gaussian fit and 25% fraction of asymmetric fission from ^{180}Hg.

In a further step we used the empirical model GEF [23] to compare the experimental results observed in this work. The GEF model [23] uses a large body of experimental information, to develope an empirical, global description of fission quantities. In GEF, the quantitative predictions of fission fragment yields rely on the properties of the fragment shells that define quantum oscillators in mass asymmetry and charge polarisation on the fission path. The positions and shapes of the fission valleys of standard fission channels [24] were obtained by fitting the structures in the measured mass distributions. The potential at elongation is calculated as the sum of the macroscopic potential and the shell effects. Although GEF is not intended for nuclei lighter than Pb, the experimental M_R distribution observed for the ^{40}Ca+^{142}Nd reaction at E^*_s=22.8 MeV has been compared with the GEF predictions for the fission of ^{182}Hg in Fig. 6 (a). The model predictions are in good agreement with the experimental results in terms of the mass centroids, peak to valley ratio and the FWHM of the mass-asymmetric peaks. The model predictions at different E^*_s values for the fission of ^{182}Hg are shown in Fig. 6 (b). It is quite clear that the distribution becomes a single Gaussian-like form at higher excitation energy for ^{182}Hg, resulting from the weakening of shell effects at such high excitations. The experimental M_R distributions obtained for the fission of ^{195}Hg in the ^{13}C+^{182}W reaction at E^*_s= 23.0 and 28.6 MeV are compared with the GEF model predictions in Fig. 6 (c). The model results matches well with the experimental M_R distribution predicting a much narrower M_R distribution for the fission of ^{195}Hg compared with ^{182}Hg. However, GEF also predicts a slightly asymmetric mass-split for the fission of ^{195}Hg, which could not be explored in detail at the moment due to the limited statistics available.

Good agreement between the experimental data and GEF indicates the persistence of shell effects at excitation energies at least up to 34 MeV, consistent with the predictions of Refs. [19, 20]. The success of the GEF model to reproduce the experimental observables suggests that the asymmetric fission observed in the neutron deficient Hg region may also be explained using the same physics that is applicable in the fission of actinide nuclei. This needs further investigation.

From the present results for the ^{40}Ca+^{142}Nd reaction, it is difficult to make definitive statements about the nature of shell effects at excitation energies above E^*=33.6 MeV. Unlike the observation at E^*=33.6 MeV, the signature

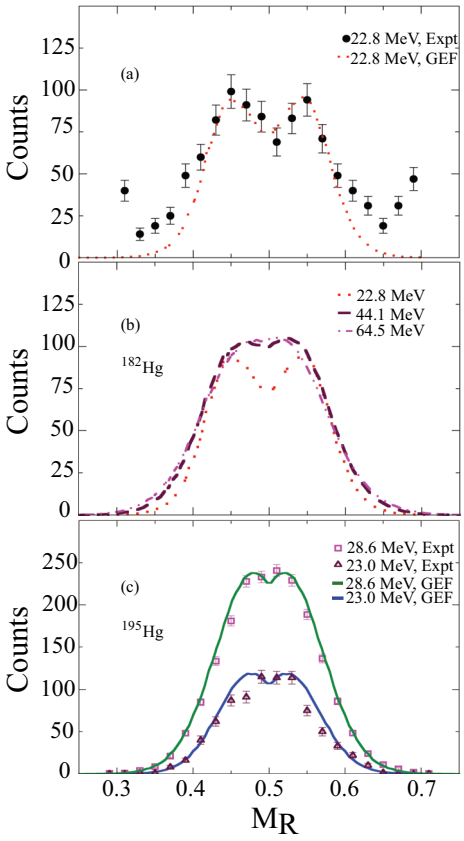

Figure 6. (a) The M_R distributions of fission fragments from the ^{40}Ca+^{142}Nd reaction at E^*_s=22.8 MeV is compared with GEF model predictions. (b) GEF predictions of the M_R distributions for the fission of ^{182}Hg at different E^*_s values. (c) GEF predictions of the M_R distributions for the fission of ^{195}Hg at different E^*_s values.

of mass-asymmetric fission is much weaker at higher excitation energies. The flat-topped M_R distribution observed at E^*=54.9 MeV and above may be indicating some asymmetric component underlying the dominant symmetric distribution. Such a flat-topped distribution has been represented by the sum of two Gaussian functions in Ref. [10] for the case of ^{36}Ar+^{144,154}Sm reactions at E^* up to 65.5 and 70.5 MeV, respectively, for the fission of ^{180}Hg and ^{190}Hg nuclei. More experimental data are required at finer energy steps to conclusively establish the excitation energy dependence of mass division in the fission of neutron-deficient Hg nuclei.

5 Summary and conclusions

In this paper we discussed the fission fragment mass-angle and mass ratio distributions for the ^{40}Ca+^{142}Nd reaction at energies around the capture barrier. Fragment mass-angle and mass ratio distributions were extracted using two-body kinematics [6]. The absence of a strong mass-angle correlations in the MAD clearly rules out the influence of fast quasifission in this reaction. The fission fragment M_R distribution shows an asymmetric mass division

with peaks centered around M_R values 0.45 and 0.55 at E^*=33.6 MeV. These M_R values are consistent with the asymmetric mass split observed in the low energy fission of ^{180}Hg in β-delayed fission experiments. Flat-topped M_R distributions have been observed at higher exciation energies, possibly indicating a small component of low E^* asymmetric fission underlying a symmetric component.

The present results are compared with the fission fragment mass distributions from the ^{36}Ar+^{144,154}Sm and ^{13}C+^{182}W reactions populating ^{180,190,195}Hg nuclei, respectively. While the fragments from ^{180,190}Hg showed signatures of asymmetric mass split, a symmetric distrbution is observed for the fission of ^{195}Hg. While the observation of mass-asymmetric fission superficially support the existence of shell effects even at high excitation energies as claimed in [10] and predicted in Refs. [19, 20], we also show empirically that the results could be explained by using a 25% fission contribution from ^{180}Hg. Even though the experimental results show similar trends as predicted in Ref. [19] in mass division, differences have been observed in the position of the mass centroids and FWHM of the peaks. On the otherhand, calculations based on an empirical model [23] reproduced the results perfectly well, supporting the influence of shell effects at compound nuclear excitation energy at least up to 34 MeV. The success of this empirical model also hints that a global description of fission may possibly be able to represent the phenomenon of fission across the nuclear chart.

Acknowledgments

The authors acknowledge support from the Australian Research Council through grants FL110100098, FT120100760, DP130101569, DP140101337, DP160101254 and DE140100784. Support for accelerator operations through the NCRIS program is acknowledged.

References

[1] R. Vandenbosch and J. R. Huizenga, *Nuclear Fission* (Academic, New York, 1973.)
[2] N. Bohr and J. A. Wheeler, Phys. Rev **56**, 426 (1939).
[3] L. Meitner, Nature **165**, 561 (1950).
[4] A. N. Andreyev, M. Huyse, and P. VanDuppen, Rev. Mod. Phys. **85**, 1541 (2013).
[5] I. F. Croall *et al.,* Nucl. Phys. **A 125**, 402 (1969).
[6] D. J. Hinde *et al.,* Phys. Rev. C **53**, 1290 (1996).
[7] R. du Rietz *et al.,* Phys. Rev. C **88**, 034611 (2013).
[8] W. J. Swiatecki *et al.,* Phys. Rev. C **71**, 014602 (2005).
[9] P. Moller *et al.,* Phys. Rev. C **79**, 064304 (2009).
[10] K. Nishio *et al.,* Phys. Lett. B, **748**, 89 (2015).
[11] E. Prasad *et al.,* Phys. Rev. C **91**, 064605 (2015).
[12] K. Ramachandran *et al.,* EPJ web of Conferences **63**, 02017 (2013).
[13] M. G. Itkis, V. N. Okolovich and G. N. Smirenkin, Nucl. Phys. **A 502**, 243c (1989).
[14] J. Elseviers *et al.,* Phys. Rev. C **88**, 044321 (2013).
[15] T. Ichikawa, A. Iwamoto and P. Moller, Phys. Rev. C **85**, 024306 (2012).
[16] M. Warda *et al.,* Phys. Rev. C **86**, 024601 (2012).
[17] A. V. Andreev *et al.,* Phys. Rev. C **88**, 047604 (2013).
[18] S. Panebianco *et al.,* Phys. Rev. C **86**, 064601 (2012).
[19] P. Moller, J. Randrup and A. J. Sierk, Phys. Rev. C **85**, 024306 (2012).
[20] J. D. McDonnel *et al.,* Phys. Rev. C **90**, 021302(R) (2014).
[21] H. Baba *et al.,* J. Phys. Soc. Jpn, **66**, 998 (1997).
[22] M. G. Itkis and A. Ya. Rusanov, Phys. Part. Nucl. **29**, 160 (1998).
[23] K. -H. Schmidt *et al.,* Nuclear Data Sheets **131**, 107 (2016).
[24] U. Brosa *et al.,* Phys. Rep. **197**, 167 (1990).